Seismic wave generation by a nonisotropic explosion source

Jeffry L. Stevens[1] and G. Eli Baker[1]

Received 29 July 2008; revised 15 June 2009; accepted 19 August 2009; published 2 December 2009.

[1] We develop a general solution for seismic wave generation by an explosion source in a spherical cavity, and then a specific solution for a point explosion source offset from the cavity center. We find that the offset causes a dipole component to the source which generates S waves and causes angular variation in P wave amplitude and shape. The S waves vanish at zero frequency but may be a sizable fraction of the P waves at frequencies of interest. We also perform a nonlinear axisymmetric calculation of an offset explosion in a spherical cavity, which causes a complex source due to cavity reverberations and generates S waves comparable to those found from the analytic solution. The solution has application to shear wave generation by decoupled explosions, and explains at least part of the shear waves observed from such explosions. Data from a pair of explosions centered and offset from the center of a spherical cavity show the expected enhancement of shear waves from the offset source.

Citation: Stevens, J. L., and G. E. Baker (2009), Seismic wave generation by a nonisotropic explosion source, *J. Geophys. Res.*, *114*, B12302, doi:10.1029/2008JB005965.

1. Introduction

[2] Decoupling of a nuclear explosion by detonation in a large cavity has been a longstanding issue for nuclear monitoring. Most previous research has focused on observation and/or prediction of the "decoupling factor," which is the amplitude ratio of the seismic signal of the tamped explosion to the seismic signal of the decoupled explosion [*Latter et al.*, 1961; *Denny and Goodman*, 1990; *Stevens et al.*, 1991a, 1991b; *Glenn and Goldstein*, 1994; *Murphy et al.*, 1997; *Stevens et al.*, 2006]. Less attention has been paid to shear wave generation by decoupled explosions, the main exception being two analyses of near field shear wave generation by the Sterling explosion [*Langston*, 1983; *Xu et al.*, 2009]. Since the most reliable discriminants for events in the magnitude range of decoupled explosions are high frequency spectral ratios of the amplitudes of the seismic shear phases Sn and Lg to Pn or Pg [*Taylor*, 1991], it is important to understand and quantify the sources of shear wave generation by decoupled explosions. In this paper we examine one such mechanism: the generation of shear waves by an explosion offset from the center of a spherical cavity.

[3] *Stevens* [1980] developed a solution for the seismic waves generated by an explosion in an arbitrarily prestressed elastic medium. In this paper, we generalize the solution to allow for cases where the explosion is nonisotropic. In particular, we consider cases where the explosion is offset from the center of the cavity so that the amplitude and arrival time of the explosion vary as a function of position on the cavity wall. The motivation for this work is that shear waves are observed from almost all explosions, including fully decoupled explosions, and one possible explanation for shear wave generation is nonspherical motion of the cavity wall in response to nonisotropic forcing by the explosion source. In the following, we model a decoupled explosion: a pressure pulse in a spherical cavity with linear elastic material outside. The examples approximately follow the Sterling decoupled explosion, a 0.38 kt explosion detonated in the 17 m cavity created by the earlier Salmon explosion. While the following solution explicitly models a decoupled explosion, it may have more general application to seismic radiation from tamped explosions in heterogeneous conditions.

2. General Solution for Variable Pressure Applied to Spherical Cavity

[4] The general solution for the seismic wavefield from a set of tractions applied to the inside of a spherical cavity is given by [*Stevens*, 1980]

$$u = -\int_{\Sigma} u \cdot T(G) \cdot \hat{n} dA + \int_{\Sigma} G \cdot T(u) \cdot \hat{n} dA - \frac{1}{i\omega}\int_{\Sigma} G \cdot T(u^*) \cdot \hat{n} dA \tag{1}$$

where Σ is the cavity surface, u on the left-hand side is the displacement at any location outside the cavity, and u inside the integral is the displacement on the cavity wall. G is the elastic Green's tensor in spherical coordinates, and T is the stress operator. The u^* is the difference in the static displacement field before and after the explosion due to changes in the static stress field, and so will vanish for a decoupled explosion where the prestress does not change, but will be nonzero for a tamped explosion with tectonic strain release. The third integral therefore represents the response of the medium to a change in prestress, the second integral represents the response of the medium to the applied stress from

[1]Science Applications International Corporation, San Diego, California, USA.

0148-0227/09/2008JB005965$09.00

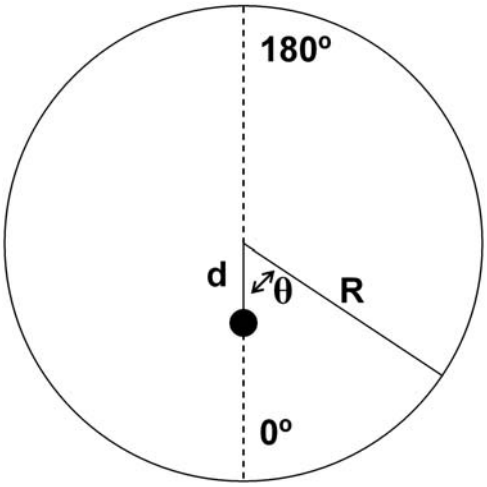

Figure 1. The explosion is offset by a distance d from the center of the cavity.

the explosion, and the first integral represents the additional motion due to the response of the cavity wall.

[5] We solve equation (1) for the case where the prestress integral vanishes and the applied stress varies at different locations on the cavity wall. We model the explosion as a pressure pulse, and assume that the applied pressure is normal to the cavity wall. In that case, the applied stress field can be expanded in vector spherical harmonics [*Morse and Feshbach*, 1953] as

$$T(u)\cdot\hat{n}=\sum_{l=0}^{\infty}\sum_{m=-l}^{l}a_{lm}(\omega,R)P_{lm}(\theta,\phi) \tag{2}$$

where using the orthogonality of the vector spherical harmonics:

$$a_{lm}(\omega,R)=\frac{2l+1}{4\pi}\frac{(l-m)!}{(l+m)!}\int_{\Sigma}P_{lm}(\theta,\phi)\cdot T(\omega,R,\theta,\phi)\cdot\hat{n}dA \tag{3}$$

By expanding the Green's tensor in equation (1) in vector spherical harmonics and again using orthogonality, we can evaluate the second integral. Defining

$$\begin{aligned}u^T&=\int_{\sum}G\cdot T(u)\cdot\hat{n}dA\\&=-i\omega\sum_{l=0}^{\infty}\sum_{m=-l}^{l}d^1_{lm}(\omega,R)P_{lm}(\theta,\phi)+d^2_{lm}(\omega,R)B_{lm}(\theta,\phi)\end{aligned} \tag{4}$$

where using the notation of *Stevens* [1980] and *Ben-Menahem and Singh* [1968]:

$$d^1_{lm}=\frac{a_{lm}}{\mu\beta}\left[\frac{g_l^{2+}(y_0)g_l^{2-}(y)}{l(l+1)}+\left(\frac{\beta}{\alpha}\right)^3 g_l^{4+}(x_0)g_l^{4-}(x)\right] \tag{5}$$

$$d^2_{lm}=\frac{a_{lm}}{\mu\beta}\left[\frac{g_l^{2+}(y_0)g_l^{3-}(y)}{l(l+1)}+\left(\frac{\beta}{\alpha}\right)^3 g_l^{4+}(x_0)g_l^{5-}(x)\right] \tag{6}$$

with $y=k_\beta r$, $x=k_\alpha r$, $y_0=k_\beta R$ and $x_0=k_\alpha R$, r the radial coordinate of the receiver point, and R the cavity radius. *Stevens* [1980] solved equation (1) for an instantaneous change in prestress with no applied stress. Except for the factor of $-i\omega$, equations (4)–(6) are expressed in the same form as the equations by *Stevens* [1980, equations 3.3 and 3.7] and so the solution is

$$u(\omega,r,\theta,\phi)=-i\omega\sum_{l=0}^{\infty}\sum_{m=-l}^{l}b^1_{lm}(\omega,r)P_{lm}(\theta,\phi)+b^2_{lm}(\omega,r)B_{lm}(\theta,\phi) \tag{7}$$

where the coefficients b^1_{lm} and b^2_{lm} are derived from d^1_{lm} and d^2_{lm} using *Stevens*' [1980] equation 3.12. Note that equation (4) gives the solution for a stress pulse applied at the cavity radius in an infinite medium with no cavity, while equation (7) includes the response of the cavity.

2.1. Solution for an Offset Explosion Source

[6] Equation (7) is the final result, giving the displacement field at any location outside the cavity in terms of the applied stress at the cavity surface, expressed as a sum of vector spherical harmonics. It is only necessary to perform the integral in equation (3) to determine the coefficients a_{lm} and the displacement field can then be calculated using the equations above. We now consider an example in which the explosion is offset from the center of the cavity as shown in Figure 1. This causes an asymmetry in the source due to the angular variation in arrival time, and the angular variation in amplitude.

[7] We assume that the pressure pulse arrival time and amplitude are only a function of θ, with no azimuthal dependence. In that case, only the m = 0 term is nonzero in the equations above, and equation (3) becomes

$$a_{l0}(\omega)=\frac{2l+1}{2}\int_0^{\pi}P_l(\cos\theta)\overline{\mathrm{P}}(\theta,\omega)\sin\theta d\theta \tag{8}$$

where P_l is the Legendre function of order l and $\overline{\mathrm{P}}(\theta,\omega)$ is the applied pressure at the cavity wall at angle θ and angular frequency ω. We also assume that the pressure eventually reaches a uniform steady state P_0, and separate the transient time and angle dependent part P_1. In the time domain,

$$\mathrm{P}(\theta,t)=[\mathrm{P}_0+\mathrm{P}_1(\theta,t-\tau(\theta))]H(t-\tau(\theta)) \tag{9}$$

where $\tau(\theta)$ corresponds to the arrival time of the shock wave on the cavity wall and $\mathrm{P}_1(\theta,\ t-\tau)$ describes its amplitude and time history. In the frequency domain, equation (9) becomes

$$\overline{\mathrm{P}}(\theta,\omega)=\left(\frac{\mathrm{P}_0}{i\omega}+\overline{\mathrm{P}}_1(\theta,\omega)\right)\exp(-i\omega\tau(\theta)) \tag{10}$$

where $\overline{\mathrm{P}}_1$ is the Fourier transform of the pressure P_1 and P_0 is a constant, the steady state pressure.

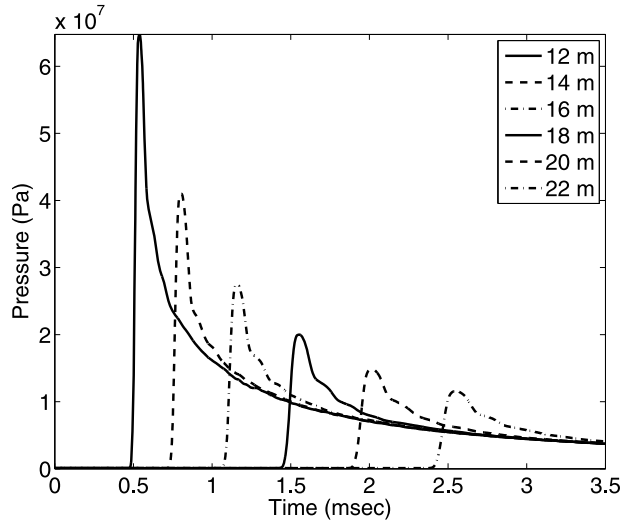

Figure 2. Pressure time history from 0.38 kt explosion in air at distances of 12–22 m.

2.2. Spherically Symmetric Calculation of the Pressure Field From an Explosion in Air

[8] To get a better idea of the form of the pressure field in equations (8)–(10), we performed a nonlinear spherically symmetric calculation of an explosion of a 0.38 kt explosion in air. The air is modeled using a tabular equation of state developed by M. Alme at the Air Force Weapons Laboratory in 1977. Figure 2 shows the pressure time histories at several locations for this calculation. Note that the time difference between peaks increases with distance as the shock wave decreases in velocity. The shock wave velocity decreases to about 5000 m/s at 17 m. Also, the shock wave becomes smaller and broader with increasing distance.

2.3. Conservation of Momentum

[9] An important constraint on the applied pressure P is that conservation of momentum requires that the total impulse on the cavity vanish. That is, forces may vary in arrival time and amplitude around the cavity wall, but cannot lead to a long-term finite impulse when integrated over the cavity wall. This condition can be expressed as follows:

$$I_x = 2\pi \int_0^{\infty} dt \int_0^{\pi} \mathrm{P}(\theta, t) \sin\theta \cos\theta d\theta = 0 \tag{11}$$

Since $\cos\theta$ is the Legendre function of order 1, this is a constraint on the dipole component of the source: the a_{10} term in equations (3) and (8). Note, however, that it does not require that the dipole vanish, only that it integrate to zero over time, or equivalently vanish at zero frequency. In the frequency domain the above condition becomes

$$\lim_{\omega\to 0} \int_0^{\pi} \overline{\mathrm{P}}(\theta, \omega) \sin\theta \cos\theta d\theta = 0 \tag{12}$$

Expanding the exponential in equation (10) for small frequencies and using the fact that the static term integrates to zero, condition (12) becomes

$$\lim_{\omega\to 0} \int_0^{\pi} \left[-\mathrm{P}_0\tau(\theta) + \overline{\mathrm{P}}_1(\theta, \omega)\right] \sin\theta \cos\theta d\theta = 0 \tag{13}$$

If we assume that the variation in arrival time can be described by a shock velocity c, so that $\tau = (R' - R)/c \approx -(d/c)\cos\theta$, the pressure can be written

$$\overline{\mathrm{P}}(\omega, \theta) = \left[\frac{\mathrm{P}_0}{i\omega} + \overline{\mathrm{P}}_1(\theta, \omega)\right] \exp(i\omega d \cos\theta/c) \tag{14}$$

Expanding $\overline{\mathrm{P}}_1$ in terms of Legendre functions,

$$\overline{\mathrm{P}}_1 = \overline{\mathrm{P}}_{10} + \overline{\mathrm{P}}_{11}\cos\theta + \ldots \tag{15}$$

and using the low frequency approximation for the exponential we get

$$\overline{\mathrm{P}}(\omega, \theta) \approx \left[\frac{\mathrm{P}_0}{i\omega} + \overline{\mathrm{P}}_{10}(\omega) + \overline{\mathrm{P}}_{11}(\omega)\cos\theta + \mathrm{P}_0\frac{d\cos\theta}{c} + \overline{\mathrm{P}}_{10}(\omega)\frac{i\omega d\cos\theta}{c} + \overline{\mathrm{P}}_{11}(\omega)\frac{i\omega d\cos^2\theta}{c}\right] \tag{16}$$

and condition (12) then gives

$$\lim_{\omega\to 0} \overline{\mathrm{P}}_{11}(\omega) + \mathrm{P}_0\frac{d}{c} = 0 \tag{17}$$

Neglecting the last term in equation (16) which varies as $(d/c)^2$, the nonvanishing coefficients in equation (3) are

$$a_{00}(\omega, R) = \left[\frac{\mathrm{P}_0}{i\omega} + \overline{\mathrm{P}}_{10}(\omega)\right]$$
$$a_{10}(\omega, R) = \overline{\mathrm{P}}_{11}(\omega) + \mathrm{P}_0\frac{d}{c} + \overline{\mathrm{P}}_{10}(\omega)\frac{i\omega d}{c} \tag{18}$$

This is a general low frequency ($\omega d/c \ll 1$) solution for the lowest order terms since we have not placed any restriction on the functional form or angular variation of the applied pressure except for its start time.

2.4. Variable Arrival Time

[10] In the simplest case, the transient pressure P_1 has the same functional form at all points on the cavity wall, differing only by start time. If we assume that P_1 has a characteristic decay time γ, so that $\mathrm{P}_1(t) = \mathrm{P}_1\exp(-\gamma t)$, then $\overline{\mathrm{P}}_{10} = \mathrm{P}_{10}/i\omega + \gamma$, and $\overline{\mathrm{P}}_{11}$ represents the momentum conserving response of the pressure field to the cavity wall. For simplicity we consider it to be a damped exponential with decay constant γ_d, so $\overline{\mathrm{P}}_{11} = \mathrm{P}_{11}/i\omega + \gamma_d$. Here P_{10} and P_{11} are constants. Condition (17) requires that $\mathrm{P}_{11} = -\mathrm{P}_0\gamma_d(d/c)$, so

$$\overline{\mathrm{P}}_{11}(\omega) = -\mathrm{P}_0\frac{d}{c}\frac{\gamma_d}{i\omega + \gamma_d} \tag{19}$$

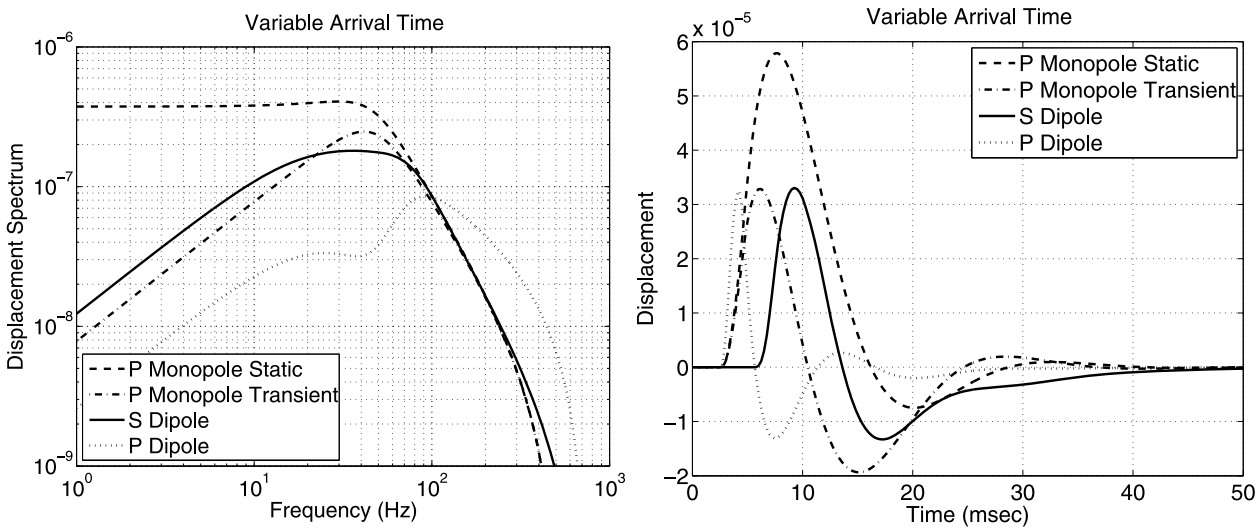

Figure 3. (left) Spectra and (right) waveforms of the monopole and two dipole terms for the angle dependent arrival time with angle independent amplitude described in the text. The dipole terms scale approximately by d/c in ms, where d is the offset from center and c is the shock velocity at the boundary.

From equation (8), the multipole coefficients are given by

$$a_{l0}(\omega) = \frac{2l+1}{2}\int_0^{\pi} P_l(\cos\theta)\left[\frac{\mathrm{P}_0}{i\omega} + \frac{\mathrm{P}_{10}}{\gamma + i\omega} - \frac{d}{c}\frac{\mathrm{P}_0\gamma_d\cos\theta}{\gamma_d + i\omega}\right] \cdot \exp\left(i\omega\frac{d}{c}\cos\theta\right)\sin\theta d\theta \tag{20}$$

The nonvanishing low frequency coefficients (equation (18)) for this case are

$$a_{00}(\omega, R) = \left[\frac{\mathrm{P}_0}{i\omega} + \frac{\mathrm{P}_{10}}{i\omega + \gamma}\right]$$
$$a_{10}(\omega, R) = i\omega\frac{d}{c}\left[\left(\frac{\mathrm{P}_0}{i\omega + \gamma_d}\right) + \left(\frac{\mathrm{P}_{10}}{i\omega + \gamma}\right)\right] \tag{21}$$

where a_{00} is the explosion monopole, which contains a static and a transient term; a_{10} is a dipole term, which in this case comes from a transient pressure of angle independent amplitude applied at the shock arrival time. At high frequencies the solution is more complicated and the coefficients must be evaluated numerically.

[11] The coefficients in equation (20) lead to three nonvanishing terms in equation (7): b_{00}, the P wave generated by the explosion monopole, b^1_{10}, the P wave generated by the dipole term, and b^2_{10}, the S wave generated by the dipole term. The P wave generated by the dipole term causes the shape of the P wave to vary with azimuth. The S wave, of course, does not exist for the monopole.

[12] Going back to equations (5)–(7), we can examine the frequency dependence of the radiated waves. In the far field, the functions $\mathrm{g}_\mathrm{l}^{2-}$ and $\mathrm{g}_\mathrm{l}^{5-}$ vanish, and the functions $\mathrm{g}_\mathrm{l}^{3-}$ and $\mathrm{g}_\mathrm{l}^{4-}$ become spherical Hankel functions with a frequency and distance dependence of $(\omega\mathrm{r})^{-1}$. In the low frequency limit, the functions $\mathrm{g}_\mathrm{l}^{2+}$ and $\mathrm{g}_\mathrm{l}^{4+}$ depend on the frequency and cavity radius as $(\omega\mathrm{R})^{\mathrm{l}-1}$, except for the l = 0 term which is proportional to ωR, so in the low frequency limit, the factors d^1_{10} and d^2_{10}, as well as b^1_{10} and b^2_{10} are proportional to $(\omega\mathrm{R})^{\mathrm{l}-2}$ and d_{00} and b_{00} are constant. From equation (7), the far field displacement is proportional to these factors times frequency. Collecting all of the factors from equations (4), (7), and (20), we find that the low frequency far field displacement from the monopole and dipole parts of the source are

$$d^1_{00} \sim i\omega a_{00}(\omega, R) = \mathrm{P}_0 + \frac{i\omega}{\gamma}\mathrm{P}_{10} \tag{22}$$

$$d^1_{10} \sim \frac{\alpha}{R}a_{10}(\omega, R) \approx i\omega\frac{\alpha}{R}\frac{d}{c}\left(\frac{\mathrm{P}_0}{\gamma_d} + \frac{\mathrm{P}_{10}}{\gamma}\right) \tag{23}$$

$$d^2_{10} \sim \frac{\beta}{R}\frac{\alpha^3}{\beta^3}a_{10}(\omega, R) \approx i\omega\sqrt{2}\frac{\alpha^3}{\beta^3}\frac{\beta}{R}\frac{d}{c}\left(\frac{\mathrm{P}_0}{\gamma_d} + \frac{\mathrm{P}_{10}}{\gamma}\right) \tag{24}$$

Including the response of the cavity increases the long period limit of b^1_{00} by about a factor of 2.5 over d^1_{00}, while the long period limit of d^1_{10} and d^2_{10} are the same as b^1_{10} and b^2_{10}.

[13] Figure 3 shows an example. We have used the coefficients in equation (20) with $\gamma = 300\mathrm{s}^{-1}$ and $\gamma_d = 150\mathrm{s}^{-1}$ which correspond approximately to the time for a shock wave to travel a cavity radius and a cavity diameter, respectively. Figure 3 shows the far-field spectra and waveforms calculated from equations (20) and (7), with $\mathrm{P}_{10} = \mathrm{P}_0$ and d/c set to 0.001. The wavefield for a different offset can be calculated approximately by multiplying the dipole waveforms by d/c (in ms) and adding to the monopole term. The monopole static and transient terms are the first and second terms in a_{00} in equation (20), respectively.

[14] With an offset of 5 m, the source is 12 m from the closest wall and 22 m from the distant wall. From Figure 2 there is a time delay of 2 ms between the opposite sides (d/c $\sim$ 1 ms), and so would generate approximately the dipole sources illustrated in Figure 3. The amplitude of the dipole terms depend on the difference in arrival time

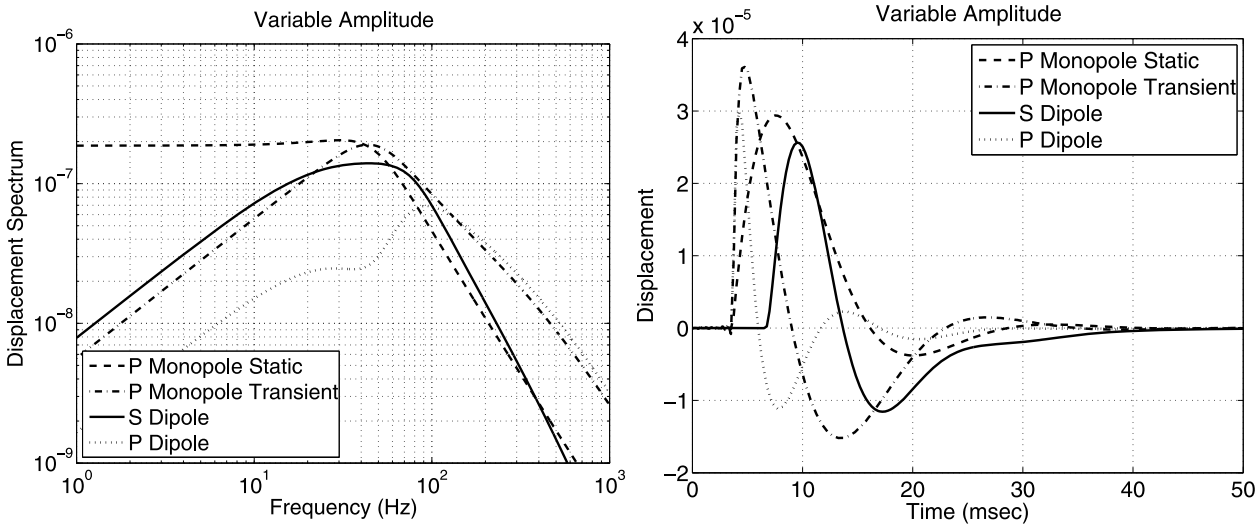

Figure 4. (left) Spectra and (right) waveforms of the monopole and two dipole terms for the angle dependent amplitude variation described in the text.

across the cavity, and therefore on the shock velocity in opposite directions. Note that this takes into account only the effect of the time delay between opposite sides, not the difference in amplitude or waveform duration.

2.5. Variable Amplitude

[15] Next, we consider the effect of amplitude variations on the cavity wall. From equation (8), the monopole and dipole coefficients for an axisymmetric source can be found by

$$a_{00} = \frac{1}{2}\int_0^{\pi} \mathrm{P}(\omega,\theta)\sin\theta d\theta \tag{25}$$

$$a_{10} = \frac{3}{2}\int_0^{\pi} \mathrm{P}(\omega,\theta)\cos\theta\sin\theta d\theta \tag{26}$$

From Figure 2, we can expect that points closer to the source will experience a higher pressure that decays faster than more distant points. So as a simple example, consider a pressure that has a value P_1 with decay time γ_1 on the side of the cavity closest to the explosion ($\theta < \pi/2$) and a value P_2 with decay time γ_2 on the side of the cavity away from the explosion $\theta > \pi/2$. This gives

$$a_{00} = \frac{1}{2}\left[\frac{\mathrm{P}_1}{\gamma_1 + i\omega} + \frac{\mathrm{P}_2}{\gamma_2 + i\omega}\right] \tag{27}$$

$$a_{10} = \frac{3}{4}\left[\frac{\mathrm{P}_1}{\gamma_1 + i\omega} - \frac{\mathrm{P}_2}{\gamma_2 + i\omega}\right] \tag{28}$$

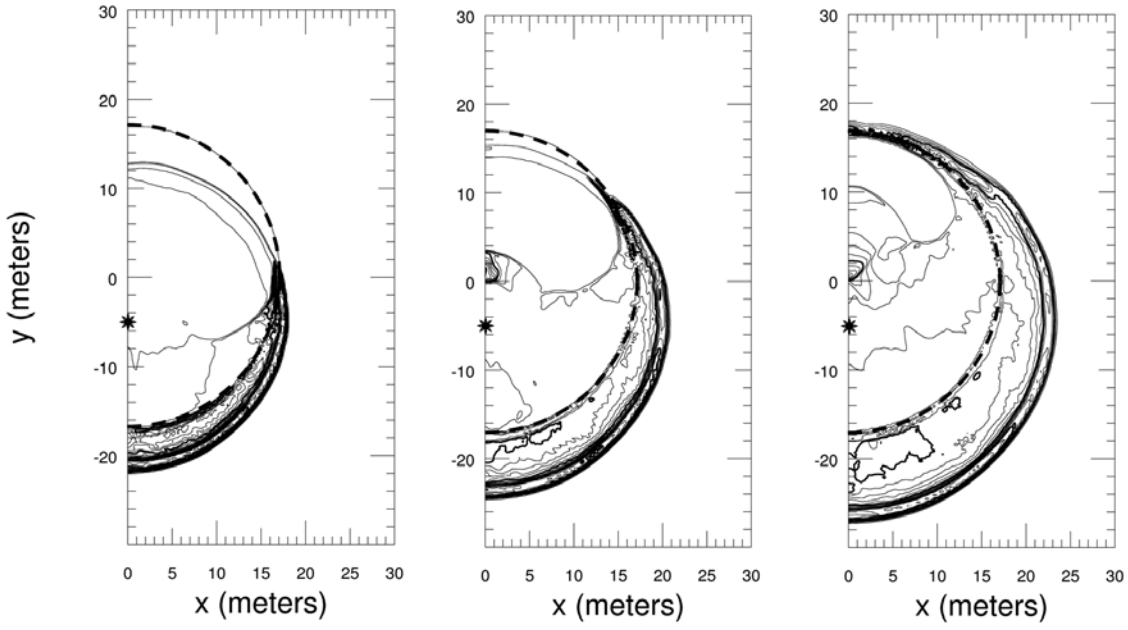

Figure 5. Pressure contours from left to right at 1.5, 2.0, and 2.5 ms. Dashed circle on the contour plot shows the cavity wall; the star shows the explosion location.

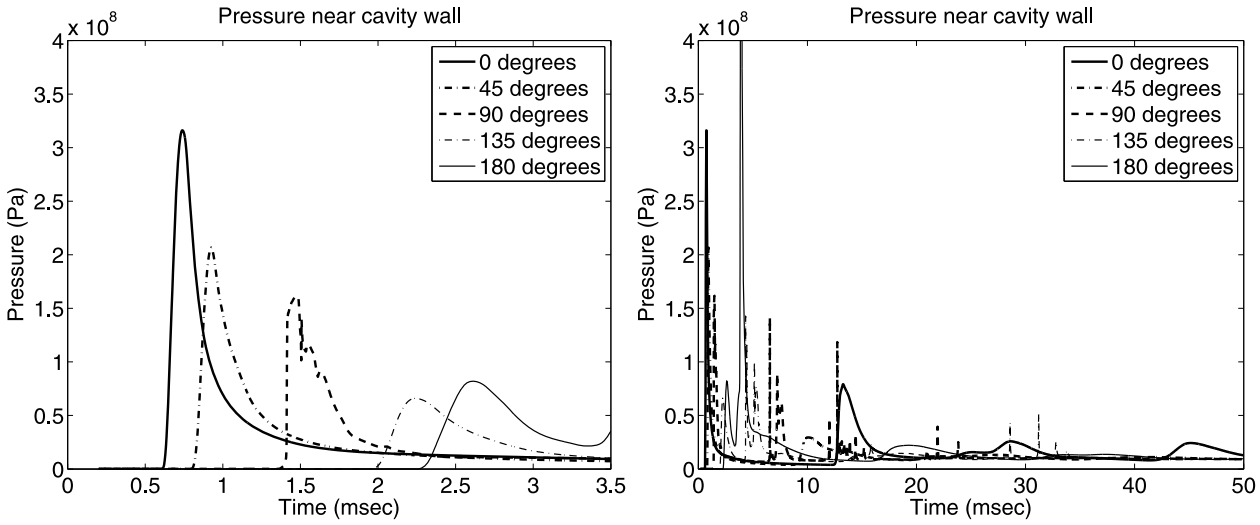

Figure 6. Pressure time histories at 5 points inside the cavity next to the wall. Zero degrees is in the direction of the explosion offset toward the bottom of the grid. (left) First 3.5 ms and (right) 50 ms.

and conservation of momentum requires that

$$\frac{P_1}{\gamma_1} = \frac{P_2}{\gamma_2} \tag{29}$$

so the pressure difference generates a dipole term, but the higher pressure applied to one side must be offset by a lower, but longer duration pressure on the other side. If there is a static pressure, this just adds $P_0/i\omega$ to a_{00}.

[16] Using the pressure calculations shown in Figure 2 and approximating the pressure applied to the two sides of the cavity with a 5 m offset by the pressures at 12 and 22 m, we get approximately for the relative pressures: $P_0 = 0.5$, $P_1 = 6.0$, $P_2 = 0.6$ (all x10^8 Pa); and for the time constants $\gamma_1 = (0.4\ \text{ms})^{-1}$, $\gamma_2 = (4\ \text{ms})^{-1}$. The far field spectra and waveforms are shown in Figure 4. The results are quite similar to those found above for the variable time delay.

2.6. Axisymmetric Calculation of an Offset Explosion in a Cavity

[17] To get a more realistic estimate of the pressure field and waveforms that would be generated by an offset explosion source, we performed a nonlinear axisymmetric calculation of an explosion in a 17 m radius air-filled cavity, offset from the center by 5 m. Calculations were performed using the Eulerian finite difference code STELLAR [*Stevens et al.*, 1991b], which was developed using the methodology of *Colella and Woodward* [1984]. Again, the explosion yield was 0.38 kt, so both the yield and cavity size corresponded to the Sterling nuclear explosion. However, we used a strong rock model exterior to the cavity to prevent the plastic yielding that occurs with salt. The calculation did not include gravity. Figure 5 shows the calculated pressure field at three times. The explosion is below the center of the cavity which corresponds to the $\theta = 0$ direction. The snapshots show the

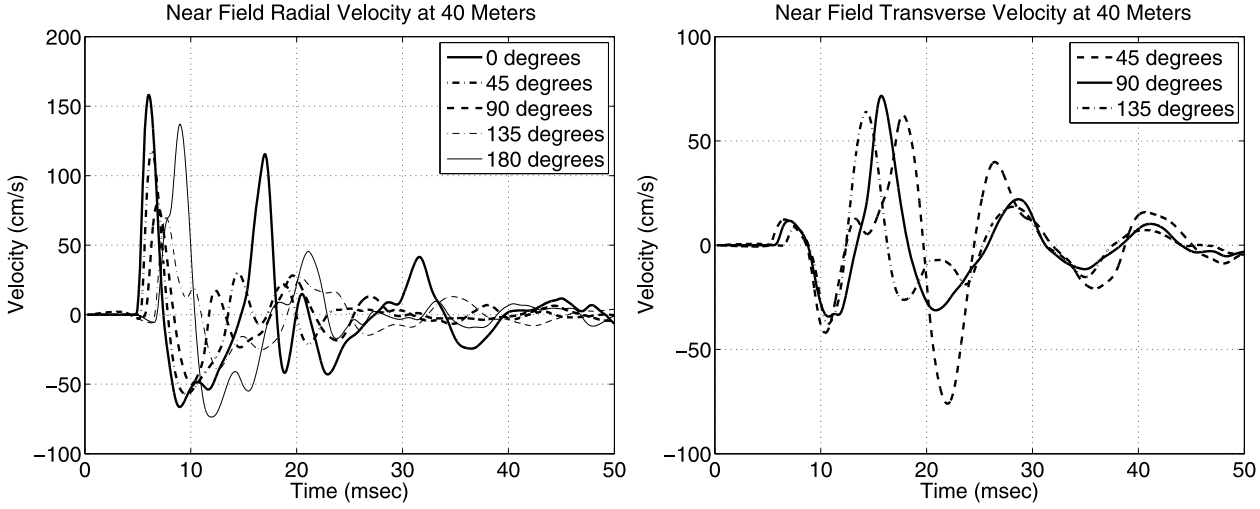

Figure 7. Radial and vertical velocity waveforms low-pass filtered at 200 Hz at a distance of 40 m from the cavity center.

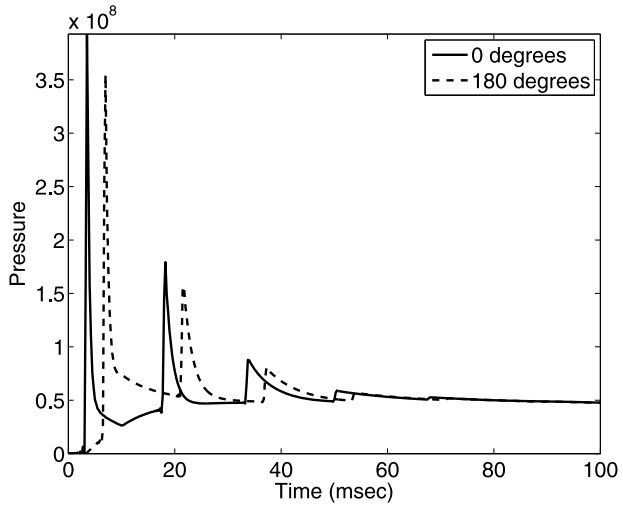

Figure 8. Pressure pulses at 0° and 180° for the multiple reverberation example.

pressure field starting after the shock wave has passed through the bottom of the cavity and continuing until it reaches the top.

[18] Figure 6 shows the pressure time histories at 5 points around the cavity just inside the cavity wall. Two time windows are shown: the first 3.5 ms and 50 ms. The pressure pulses in the first 3.5 ms are similar to the free field pulses in Figure 2, but have a larger initial peak and are more complex because of the interaction between the shock wave and the cavity wall. These are followed by a series of complex cavity reverberations that persist for quite a long time. The first reverberation at the far side of the cavity from the explosion is actually larger than the initial pressure pulse. This is caused by the reflected wave from the bottom of the cavity arriving at the top in time to interfere with the first reflection from the top. Notice in Figure 5 (right) that the reflected wave has almost reached the top. There is a large pressure spike at the top at about 4 ms.

[19] Figure 7 shows velocity waveforms at 45° increments from the offset direction to opposite direction at a distance of 40 m from the cavity center. At this distance the

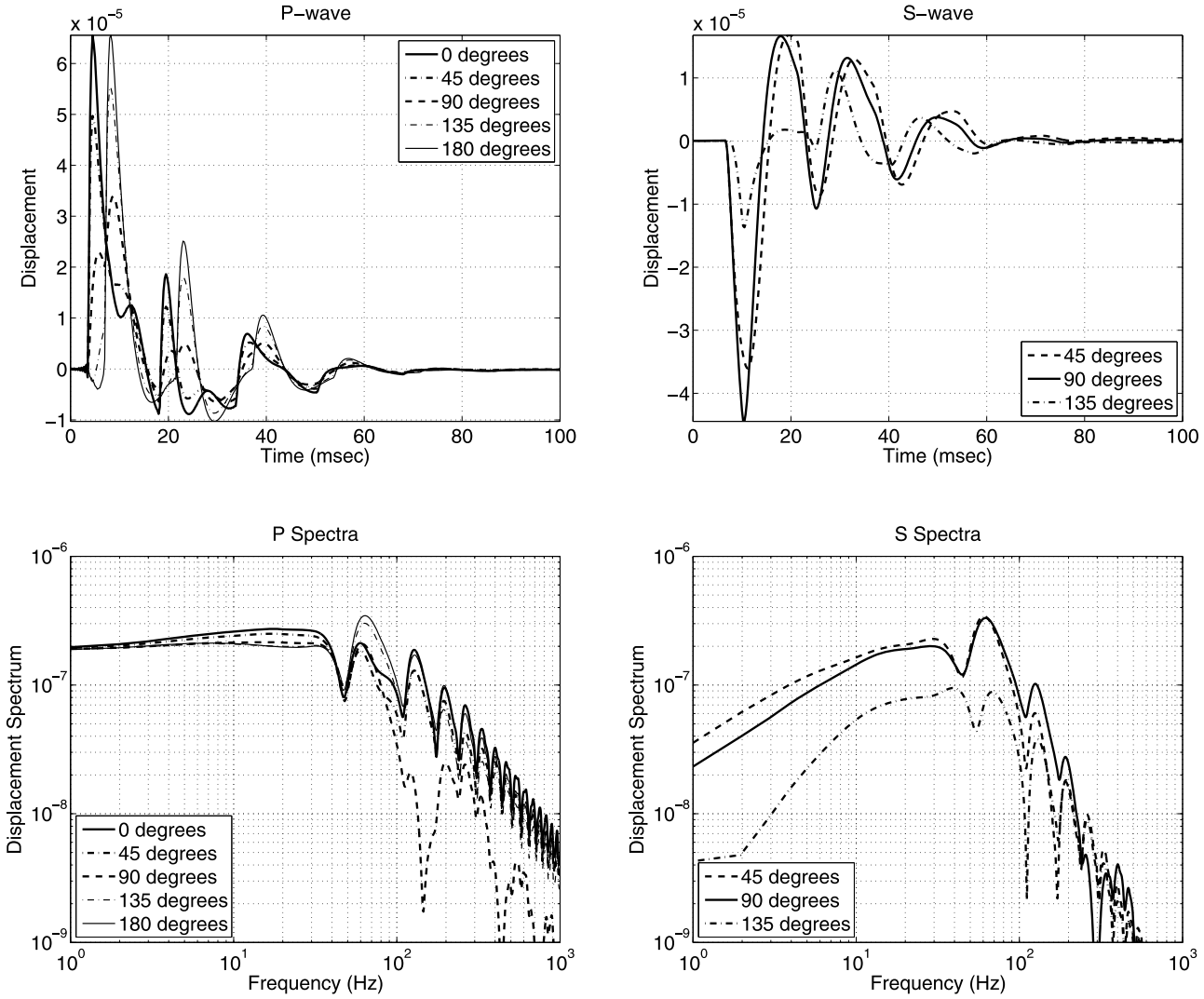

Figure 9. Far field P and S (top) waveforms and (bottom) spectra generated by the pressure pulses in Figure 8.

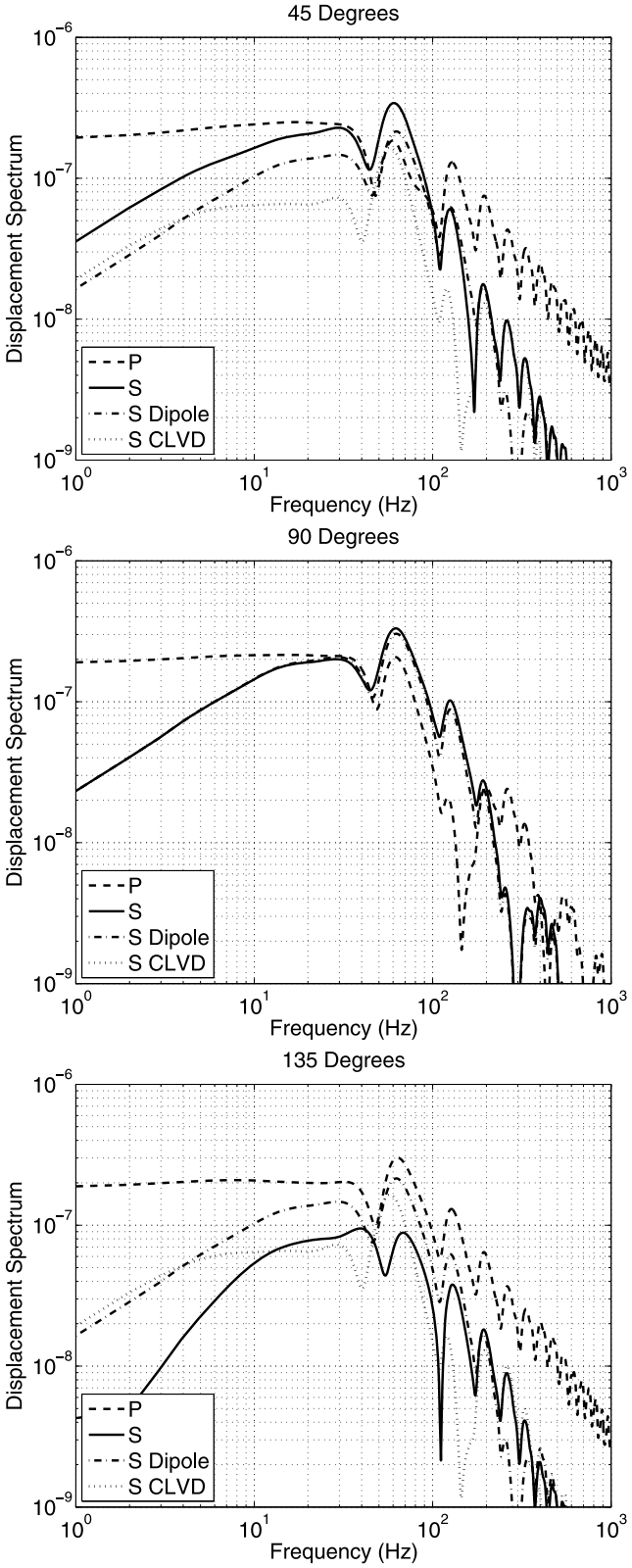

Figure 10. Composition of spectra at 3 angles: (top) 45°, (middle) 90°, and (bottom) 135°.

radial and transverse components are mixed P and S waves, but the radial is primarily P and the transverse is primarily S. The amplitude of the S phase relative to P is comparable to the offset source solutions. The waveforms are considerably more complex because of the greater complexity of the pressure field in the cavity, and because 40 m is still in the near field for the waveforms.

2.7. Multiple Reverberations

[20] As a final example we consider the effect of multiple reverberations similar to those seen in the calculation above. The pressure pulses are stronger at the ends of the cavity, and decline in amplitude with each reverberation. We model the pressure field as a series of transient pressure pulses on each half of the cavity with maximum amplitude at zero and π, varying as cos θ:

$$\overline{\mathrm{P}}(\theta,\omega) = \sum_{n=1}^{N} \frac{\mathrm{P}_n \exp(-i\omega t_n)}{\gamma_n + i\omega} \cos\theta \; 0 < \theta \le \frac{\pi}{2} \tag{30}$$

$$\overline{\mathrm{P}}(\theta,\omega) = -\sum_{m=1}^{N} \frac{\mathrm{P}_m \exp(-i\omega t_m)}{\gamma_m + i\omega} \cos\theta \; \frac{\pi}{2} < \theta \le \pi \tag{31}$$

where the times correspond to successive reverberation times on opposite sides of the cavity. We also apply the final static pressure with the first pressure pulse on each side, and a compensating decaying pressure to conserve momentum as discussed in section 2.4. For ease of comparison, we use the same values of P_0, P_1 and γ_1 as in the variable amplitude case. Multipole coefficients through l = 4 were calculated. With $N = 1$, corresponding to a single pressure pulse on each side, the results are similar to the earlier examples. With multiple reverberations, however, the waveforms are longer in duration and have more low frequency content. For this example, we use 10 reverberations, with P decaying exponentially with time as $\exp(-\gamma_0 t)$ with γ_0 = 80, and additionally decreasing 10% with each reflection. Decay coefficients follow equation (29) for each successive pair of pressure pulses on opposite sides of the cavity. Figure 8 shows the pressure at opposite ends of the cavity. The momentum compensating static pressure correction causes the early time offset in the pressure on opposite sides of the cavity.

[21] Figure 9 shows the P and S waves at 45°, 90°, and 135°. Notice the increase in low frequency amplitude and pulse duration compared to the earlier examples.

[22] Figure 10 shows the spectra at 3 angles divided into its multipole components. In the earlier examples the l = 2 (CLVD) component was negligible, but in this case because we made the pressure at the ends of the cavity larger than the sides, the CLVD component is significant, in fact comparable to the dipole component. Notice that at 45° the dipole and CLVD components add constructively, increasing S, while at 135° they add destructively, substantially reducing S at low frequencies. The CLVD component has a node at 90°, so only the dipole component contributes to S at that angle. As shown in Figure 9, the radiation pattern of the combined waveform appears to be that of a dipole since the first motion is in the same direction at all three angles.

3. Discussion and Conclusions

[23] We have developed a general solution for seismic wave generation by an explosion source in a spherical

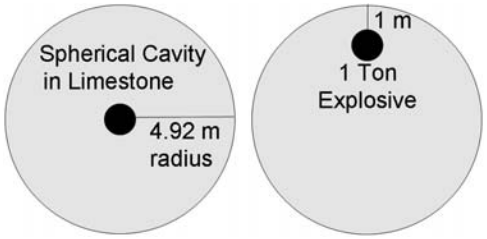

Figure 11. Configuration of Kirghizia explosions at the center and upper edge of a spherical cavity.

cavity, and evaluated the solution for a point explosion offset from the cavity center. This offset causes a dipole component to the source which generates S waves and causes angular variation in P wave amplitude and shape. *Zhao and Harkrider* [1992] also found a dominant dipole component for an offset explosion embedded in a solid sphere. Depending on the distribution of the pressure field, the CLVD component to the source may also be significant. By conservation of momentum, the S waves must vanish at zero frequency but they may be a sizable fraction of the P waves at frequencies of interest. We also performed a nonlinear axisymmetric calculation of an offset explosion in a spherical cavity. This leads to a much more complex pressure field on the cavity wall and correspondingly more complex near field waveforms. However, the calculated S waves are comparable in amplitude (relative to P) to those found from the analytic solution. The longer duration of the source when cavity reverberations are included increases the low frequency content of the S waves.

[24] Two chemical explosion tests with geometry very similar to that modeled in this paper provide a comparison with our theoretical results (Figure 11). The tests were conducted in Kirghizia in 1960 as part of a series described by *Murphy et al.* [1997]. In one test, 1 t of explosives was detonated in the center of a spherical cavity. In another, 1 t of explosives was detonated near the upper edge of the same cavity. Both were recorded at 5 km on the same instrument. The identical source and receiver locations make this a particularly good example. S waves may be generated by a variety of phase conversion and scattering processes, making isolation of source effects difficult in many cases, but here we can confidently attribute differences to the source offset. Based on the analysis given here, we would expect to see enhanced shear waves at higher frequencies from the off-center explosion. The low frequency spectra depend on the duration of the cavity reverberations, which is not well determined, but using the analysis presented in section 2.5 for the angle dependent amplitude with the same parameters, except for the smaller 4.92 m cavity and material properties appropriate for limestone (P velocity 6000 m/s, S 3750 m/s, density 2700 kg/m^3), leads to the spectra shown in Figure 12 for the offset source at a takeoff angle of 90°. Note that although both the P and S spectra peak at high frequencies, and the S spectrum goes to zero at zero frequency, the P and S spectra are comparable in amplitude at about 10 Hz. Figure 13 shows data for the centered and offset explosions recorded at 5 km, filtered in two bands from 2 to 8 Hz and 8–14 Hz and normalized by the vertical P wave amplitude, as the off-center explosion was less decoupled. The data clearly show the expected enhancement of S waves in the 8–14 Hz frequency band for the offset source relative to the centered source.

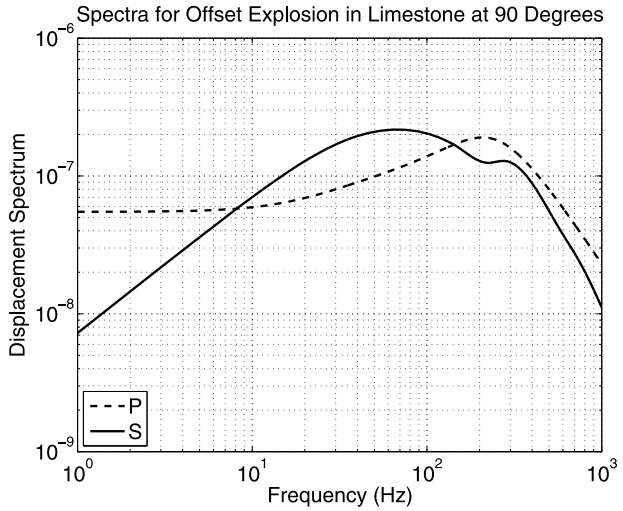

Figure 12. Calculated P and S spectra at 90° (horizontally) from the offset source configuration shown in Figure 11.

[25] The calculations performed earlier in this paper used parameters modeled after the Sterling explosion: 0.38 kt yield in a 17 m cavity. The Sterling explosion was conducted in the cavity generated by the earlier 5.3 kt explosion Salmon in a salt dome. The cavity had a flat bottom due to melt that filled in approximately 7 m at the base of the cavity [*Healy et al.*, 1971]). Consequently the bottom of the cavity was closer to the explosion source than the top, and so the calculations here are relevant to that explosion, although we are addressing the more general problem of shear wave generation and P wave variations caused by an offset explosion source. A more complete treatment of the shear waves generated the Sterling explosion including calculations with the flat bottom using a realistic salt model is given by *Xu et al.* [2009].

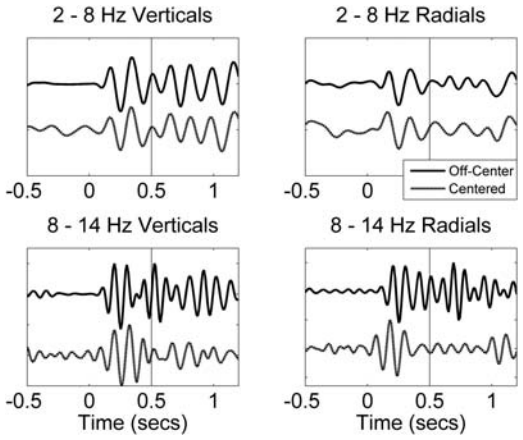

Figure 13. (left) Vertical and (right) radial components of data from the centered and offset Kirghizia explosions filtered from (top) 2 to 8 Hz and (bottom) 8–14 Hz, scaled by the maximum vertical component amplitude. Increased shear waves are apparent in the higher frequency seismograms from the offset source.

[26] Although the solution given above strictly applies only to decoupled explosions, it may have relevance to tamped explosions as well. A tamped explosion is characterized by a pressure pulse that propagates through the surrounding medium causing nonlinear deformation of rock out to the elastic radius, which is an order of magnitude larger than the cavity radius. The tamped explosion source can also be expanded in spherical harmonics as with the decoupled source. Empirical explosion source models such as the *Mueller and Murphy* [1971] model parameterize the explosion source as a spherically symmetric pressure pulse applied at the elastic radius. Propagation through heterogeneous media, as well as the effects of the free surface and gravity, cause angular variations in the explosion source function, so the tamped explosion source may be more accurately characterized as a multipole source. The conservation of momentum constraints apply to a tamped source as well, and so the dipole component of the source must always vanish in the long period limit, however it may cause shear wave generation at higher frequencies of interest. In the examples given above, the CLVD source also vanished in the long period limit. This is because the final state of the pressurized cavity is uniform, however this is not necessarily the case for a tamped source and the CLVD (or other configurations of the $l = 2$ multipole source including $m \neq 0$) may have a nonvanishing static limit for a tamped explosion caused by nonspherical permanent deformation.

[27] **Acknowledgments.** We thank Steve Day for pointing out the conservation of momentum condition. This work was supported by Air Force Research Laboratory contract FA8718-06-C-0007.

References

Ben-Menahem, A., and J. Singh (1968), Eigenvector expansions of Green's Dyads with applications to geophysical theory, *Geophys. J. R. Astron. Soc.*, *52*, 65–96.

Colella, P., and P. R. Woodward (1984), The Piecewise Parabolic Method (PPM) for Gas-Dynamical Simulations, *J. Comput. Phys.*, *54*, 174–201, doi:10.1016/0021-9991(84)90143-8.

Denny, M. D., and D. M. Goodman (1990), A case study of the seismic source function: Salmon and Sterling reevaluated, *J. Geophys. Res.*, *95*(B12), 19,705–19,723, doi:10.1029/JB095iB12p19705.

Glenn, L., and P. Goldstein (1994), Seismic decoupling with chemical and nuclear explosions in salt, *J. Geophys. Res.*, *99*(B6), 11,723–11,730, doi:10.1029/94JB00497.

Healy, J. H., C.-Y. King, and M. E. O'Neill (1971), Source parameters of the Salmon and Sterling nuclear explosions from seismic measurements, *J. Geophys. Res.*, *76*, 3344–3355, doi:10.1029/JB076i014p03344.

Langston, C. A. (1983), Kinematic analysis of strong motion P and SV waves from the Sterling event, *J. Geophys. Res.*, *88*, 3486–3497, doi:10.1029/JB088iB04p03486.

Latter, A. L., R. E. Lelevier, E. A. Martinelli, and W. G. McMillan (1961), A method of concealing underground nuclear explosions, *J. Geophys. Res.*, *66*, 2929–2936, doi:10.1029/JZ066i009p02929.

Morse, P. M., and H. Feshbach (1953), *Methods of Theoretical Physics*, McGraw-Hill, New York.

Mueller, R. A., and J. R. Murphy (1971), Seismic Characteristics of Underground Nuclear Detonations, I: Seismic Spectrum Scaling, *Bull. Seismol. Soc. Am.*, *61*, 1675–1692.

Murphy, J. R., I. O. Kitov, N. Rimer, V. V. Adushkin, and B. W. Barker (1997), Seismic characteristics of cavity decoupled explosions in limestone: An analysis of Soviet high explosive test data, *J. Geophys. Res.*, *102*, 27,393–27,405, doi:10.1029/97JB02475.

Stevens, J. L. (1980), Seismic radiation from the sudden creation of a spherical cavity in an arbitrarily prestressed elastic medium, *Geophys. J. R. Astron. Soc.*, *61*, 303–328.

Stevens, J. L., J. R. Murphy, and N. Rimer (1991a), Seismic source characteristics of cavity decoupled explosions in salt and tuff, *Bull. Seismol. Soc. Am.*, *81*, 1272–1291.

Stevens, J. L., N. Rimer, J. R. Murphy, T. G. Barker, E. Bailey, E. J. Halda, W. Proffer, S. H. Rogers, and B. Shkoller (1991b), Simulation of seismic signals from partially coupled nuclear explosions in spherical and ellipsoidal cavities, S-Cubed final report SSS-FR-91–12735, August.

Stevens, J. L., S. Gibbons, N. Rimer, H. Xu, C. Lindholm, F. Ringdal, T. Kvaerna, and J. R. Murphy (2006), Analysis and simulation of chemical explosions in nonspherical cavities in granite, *J. Geophys. Res.*, *111*, B04306, doi:10.1029/2005JB003768.

Taylor, S. R. (1991), Regional seismic observations from NTS explosions, *Explosion Source Phenomenology*, *Geophys. Monogr. Ser.*, vol. 65, edited by S. Taylor, H. Patton, and P. Richards, pp. 185–196, AGU, Washington, D. C.

Xu, H., J. L. Stevens, and G. E. Baker (2009), An analysis of shear waves generated by the Sterling explosion, *J. Geophys. Res.*, *114*, B03307, doi:10.1029/2008JB005966.

Zhao, L., and D. G. Harkrider (1992), Wave fields from an off-center explosion in an embedded solid sphere, *Bull. Seismol. Soc. Am.*, *82*, 1927–1955.

G. E. Baker and J. L. Stevens, Science Applications International Corporation, 10260 Campus Point Dr., San Diego, CA 92121, USA. (Jeffry.L.Stevens@saic.com)